The Journal of Chemical Physics

Effects of interfaces on structure and dynamics of water droplets on a graphene surface: A molecular dynamics study

Cite as: J. Chem. Phys. **154**, 164704 (2021); https://doi.org/10.1063/5.0046817
Submitted: 07 February 2021 . Accepted: 05 April 2021 . Published Online: 23 April 2021

Manish Maurya, Atanu K. Metya, Jayant K. Singh, Shinji Saito, et al.

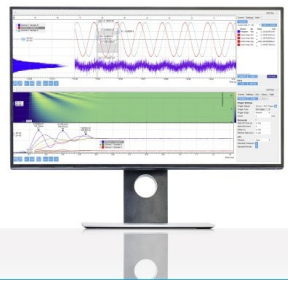

AIP Publishing

The Journal of Chemical Physics ARTICLE scitation.org/journal/jcp

Effects of interfaces on structure and dynamics of water droplets on a graphene surface: A molecular dynamics study

Cite as: J. Chem. Phys. 154, 164704 (2021); doi: 10.1063/5.0046817
Submitted: 7 February 2021 • Accepted: 5 April 2021 •
Published Online: 23 April 2021

Manish Maurya,[1] Atanu K. Metya,[2] Jayant K. Singh,[3] and Shinji Saito[1,4,a)]

AFFILIATIONS

[1]Department of Theoretical and Computational Molecular Science, Institute for Molecular Science, Myodaiji, Okazaki, Aichi 444-8585, Japan
[2]Department of Chemical and Biochemical Engineering, Indian Institute of Technology Patna, Bihar 801106, India
[3]Department of Chemical Engineering, Indian Institute of Technology Kanpur, Kanpur 208016, India
[4]The Graduate University for Advanced Studies, Myodaiji, Okazaki, Aichi 444-8585, Japan

[a)]**Author to whom correspondence should be addressed:** shinji@ims.ac.jp

ABSTRACT

The structure and dynamics of water droplets on a bilayer graphene surface are investigated using molecular dynamics simulations. The effects of solid/water and air/water interfaces on the local structure of water droplets are analyzed in terms of the hydrogen bond distribution and tetrahedral order parameter. It is found that the local structure in the core region of a water droplet is similar to that in liquid water. On the other hand, the local structure of water molecules at the solid/water and air/water interfaces, referred to as the interface and surface regions, respectively, consists mainly of three-coordinated molecules that are greatly distorted from a tetrahedral structure. This study reveals that the dynamics in different regions of the water droplets affects the intermolecular vibrational density of states: It is found that in the surface and interface regions, the intensity of vibrational density of states at ~50 cm^{-1} is enhanced, whereas those at ~200 and ~500 cm^{-1} are weakened and redshifted. These changes are attributed to the increase in the number of molecules having fewer hydrogen bonds in the interface and surface regions. Both single-molecule and collective orientation relaxations are also examined. Single-molecule orientation relaxation is found to be marginally slower than that in liquid water. On the other hand, the collective orientation relaxation of water droplets is found to be significantly faster than that of liquid water because of the destructive correlation of dipole moments in the droplets. The negative correlation between distinct dipole moments also yields a blueshifted libration peak in the absorption spectrum. It is also found that the water–graphene interaction affects the structure and dynamics of the water droplets, such as the local water structure, collective orientation relaxation, and the correlation between dipole moments. This study reveals that the water/solid and water/air interfaces strongly affect the structure and intermolecular dynamics of water droplets and suggests that the intermolecular dynamics, such as energy relaxation dynamics, in other systems with interfaces are different from those in liquid water.

I. INTRODUCTION

Water is one of the prerequisites for life and is the most common solvent in physicochemical processes.[1,2] Despite having a simple molecular structure, water molecules can form strong hydrogen bonds (HBs) with each other in liquid water. As seen in ice, water molecules tend to form a local tetrahedral structure. However, owing to thermal fluctuations, local structures in liquid water are distorted. As a result, liquid water shows spatially and temporally complex fluctuations and numerous anomalous properties are found, such as a sharp change in the thermodynamic response function with decreasing temperature.[3] It is now considered that the anomalous thermodynamic properties of water are related to fluctuations between low- and high-density liquid states.[4–13]

It is known that structural, dynamical, and thermodynamic properties of liquid water are strongly influenced by intermolecular HB interactions. Thus, when the intermolecular interactions among water molecules are interrupted by solvation, the structural and dynamical properties of these molecules in an aqueous solution are altered,[14–18] an example being the acceleration or retardation of collective orientation relaxation (COR) of aqueous solutions. Furthermore, hydration of proteins also changes the properties of water. For example, the density of water molecules present at the surface of a protein is found to be greater than that of liquid water.[19] In this context, the fast librational and reorientational dynamics of water molecules in the hydration layer of proteins have also been explored.[20]

In addition to the presence of solutes, interfaces and surfaces also affect the properties of water. In this regard, the structure and intramolecular dynamics of water interfaces have been intensively investigated using surface-specific spectroscopy. In particular, one- and two-dimensional vibrational sum-frequency generation (SFG) spectroscopies have been applied to intramolecular vibrations of water at air/water interfaces.[21–26] Furthermore, water molecules at the solid–water interface have also been a subject of immense scientific interest due to its importance in a broad range of physicochemical and technological processes, such as surface wettability,[27,28] lubrication,[29,30] and capillary condensation.[31]

A water droplet on a solid surface is a system with both air/water and solid/water interfaces. In this context, the contact angle of water droplets has been investigated both theoretically and experimentally,[32–35] which plays an important role in wetting kinetics of water droplets on a solid interface. The behavior of water droplets in the presence of an electric field has also been studied and forms the basis for techniques such as inkjet and electrostatic painting and the manufacture of nanoscale structures.[36–39] However, not much is known about structural and dynamical properties at the molecular level of water droplets on a solid surface.

In this study, we investigate these properties of water droplets on a bilayer graphene surface at the molecular level using molecular dynamics (MD) simulations. First, we examine the effect of solid–water interaction strength on the local structure of water molecules in water droplets on a graphene surface. Then, we investigate the dynamical properties in terms of the intermolecular vibrational density of states (vDOS). We find that the dynamics in the core region of a water droplet are very similar to those in liquid water. On the other hand, the intermolecular vibrational vDOS shows a redshift in the water/solid and water/air interface regions owing to fewer HBs being present. We study both single-molecule and collective orientation relaxations of water droplets. It is known that collective orientation relaxation (COR) is slower than single-molecule orientation relaxation (SMOR) in liquid water. However, the present study reveals that COR in water droplets is much faster than SMOR because of a negative correlation between dipole moments. It is also clarified that the peak of the librational motion in the absorption spectrum of a water droplet is blueshifted owing to the negative correlation of distinct dipole moments. We also find that the structure and dynamics of the water droplets are sensitive to the water–graphene interaction.

The remainder of the paper is organized as follows: The computational details are outlined in Sec. II. The results are discussed in Sec. III, and conclusions are given in Sec. IV.

II. COMPUTATIONAL DETAILS

We perform classical MD simulations for water droplets on a graphene surface. The water droplets are modeled using the TIP4P/2005 rigid water model, which is known to correctly reproduce the structural and dynamical properties of liquid water.[40] Initially, a cube of one thousand water molecules is placed in the middle of the graphene surface to model a water droplet. After a few steps of MD simulation, this water cube takes the form of a droplet, as shown in Fig. 1.

The flat solid surface is modeled using the bilayer (AA stacking) of graphene sheets with an interlayer spacing of 3.4 Å and a C–C bond length of 1.42 Å. The graphene sheets are considered to be representative of a flat solid surface with different interaction strengths. The carbon atoms of the graphene sheets are modeled using the AMBER96 force field.[41] A single graphene sheet is very flexible, and thus, ripples on the graphene surface are found to have some effect on the wettability of a water droplet.[42] However, the effect is negligible in the current case as the number of layers considered in this work does not cause ripples and can be considered as a rigid substrate as also considered by earlier workers.[43] The interaction potential between a carbon atom of the graphene surface and a water molecule is taken from the work of Werder *et al.*[43] The potential parameters are listed in Table I. The Lennard-Jones (LJ) potential depth between a carbon atom and the water droplet (ε_{C-O} in kcal/mol) is increased by 20%, 40%, and 60% to examine the effect of enhanced interaction strength with the graphene surface. The droplet size on the surface depends on the strength of interaction with the surface and reaches a radius of 1–3 nm. The simulations are performed using the LAMMPS software[44] in the *NVT* ensemble at 300 K with periodic boundary conditions and the particle–particle–particle–mesh (PPPM) treatment of long-range electrostatic interactions. A cutoff of 14 Å is used for nonbonded interaction, and the SHAKE algorithm is used to constrain the bonds between the hydrogen and oxygen atoms of water molecules. Although the periodic boundary conditions and PPPM are used in this study, the interactions between water droplets are effectively removed by considering a large simulation cell compared to the droplet size. The length of the simulation is 30 ns with a time step of 1 fs. We confirmed that

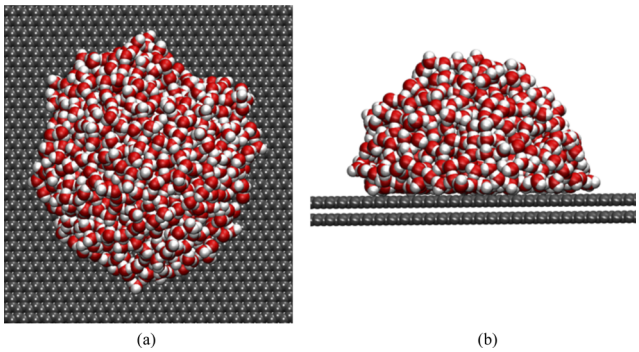

FIG. 1. Top (a) and side (b) views of the graphene surface and water droplet at 300 K. For clarity, the full extent of the system is not shown. The carbon atoms of the graphene sheet are shown in gray and the hydrogen and oxygen atoms of the water droplet in white and red, respectively.

TABLE I. Lennard-Jones force field parameters for graphene–water interaction.

Atom pair	ε (kcal/mol)	σ (Å)
C–C	0.086	3.4
C–O	0.094	3.19

the system is equilibrated within 20 ns by analyzing the fluctuation in the total energy of the system. For the data analysis, the trajectories from the last 10 ns run are stored at an interval of 10 fs. In addition, we perform an independent simulation of the liquid water in the *NVT* ensemble to compare the results of the water droplets. The simulation is carried out in a cubic box containing 1000 water molecules of a density of 1 g/cc at 300 K. The other simulation details are the same as the water droplets.

III. RESULTS AND DISCUSSION

A. Structural analysis of water droplet

Figure 2 shows the distribution of water molecules in the direction perpendicular to the graphene surface with different graphene–water LJ interactions. The shape of the water droplet depends on the strength of its interaction with the graphene surface. In the case of usual interaction (ε_{C-O} = 0.094 kcal/mol) with the graphene surface (red line), the water droplet does not spread much on the surface, resulting in a broad distribution of molecules in the direction perpendicular to the surface. Water droplets with stronger interactions with the graphene surface show a larger peak in the distribution of atoms near the surface (at low z), indicating the spreading of molecules on the surface. As the interaction with the surface increases, the intensity of the peak increases. The snapshots in Fig. 3 indeed show changes in the shape of the droplet in various graphene–droplet systems. We examine the contact angle of the water droplets by using a graphical binning approach.[45,46] As shown in Table II, the contact angle decreases with increasing water–graphene interaction. The present result is in good agreement with previous results.[43,47]

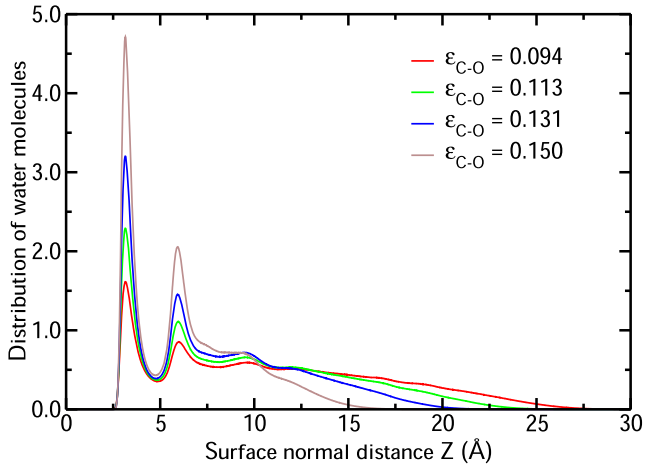

FIG. 2. Number distribution of oxygen atoms in surface–droplet systems. ε_{C-O} represents the LJ cross-interaction potential. The red line shows the result with the usual interaction, and the green, blue, and brown lines correspond to 20%, 40%, and 60% enhancement in the LJ potential (in kcal/mol), respectively.

We now examine preferred orientations of water molecules in the first layer of the droplet on the graphene surface. Here, we analyze the orientation of water molecules based on two angles: One is the angle α between the H–H vector (the line joining the two hydrogen atoms) and the normal to the graphene surface, and the other is the angle β between the dipole moment and the normal to the graphene surface. Figures 4(a) and 4(b) show the two-dimensional probability distributions of α and β in the systems having the usual and 60% enhanced graphene–water interactions, respectively. The result shows that water molecules orient themselves preferentially in three different orientations: The most preferable orientation is (α, β) = (~90°, ~100°), and the others are (α, β) = (~40°, ~55°) and (α, β) = (~140°, ~55°), respectively. The present result on the preferred orientation distribution of water droplets on a graphene surface is consistent with previous studies.[48,49] Figure 4(c) shows that the distribution of the H–H vector parallel to the graphene surface increases with increasing water–graphene interaction. Figure 4(d) shows that

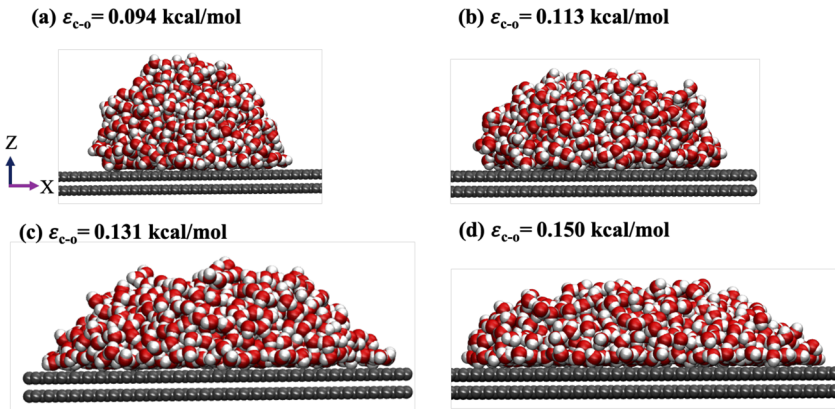

FIG. 3. Snapshots of the water droplet having (a) the usual interaction and (b) 20%, (c) 40%, and (d) 60% enhanced interactions. For clarity, the full extent of the system is not shown.

TABLE II. Contact angle of the water droplet for different water–graphene interactions.

ε_{C-O} (kcal/mol)	0.094	0.113	0.131	0.150
Contact angle (deg)	95 ± 3	76 ± 2	53 ± 1	34 ± 1

the bimodality of the distribution of the angle between the dipole moment and the surface normal becomes more intense with increasing water–surface interaction. Furthermore, it is found that the total dipole moment of water molecules in the first layer points upward with respect to the normal to the graphene surface. In addition, the distributions of orientation do not change much by changing the interaction strength between the water droplet and graphene surface.

Next, we examine the distribution of the number of HBs per molecule in the water droplets and liquid water. Two criteria are used for identifying an HB between any two water molecules: The distance $r_{O\cdots O}$ between the oxygen atoms of both molecules should be ≤3.4 Å, and the angle $\theta_{H\cdots O}$ should be ≤30° (here, a dotted line denotes an intermolecular vector, whereas a solid line denotes an intramolecular vector).[50] Figure 5(a) presents the fraction of water molecules forming a particular number of HBs in the water droplets and liquid water. It shows that ~55% are four-coordinated water molecules in liquid water, whereas ~45% of water molecules are involved in forming four HBs in the water droplets. The fraction of water molecules forming a higher coordination number, i.e., ≥4, decreases as the interaction between water and the graphene surface increases, while the fraction forming a lower coordination number, i.e., ≤3, increases with increasing water–graphene interaction. Thus, the nature of the graphene–water interaction affects the coordination number of water molecules in the droplet in comparison to that of liquid water. However, the change in the distributions of the fraction of HBs is not much by changing the interaction strength between the water droplet and graphene surface.

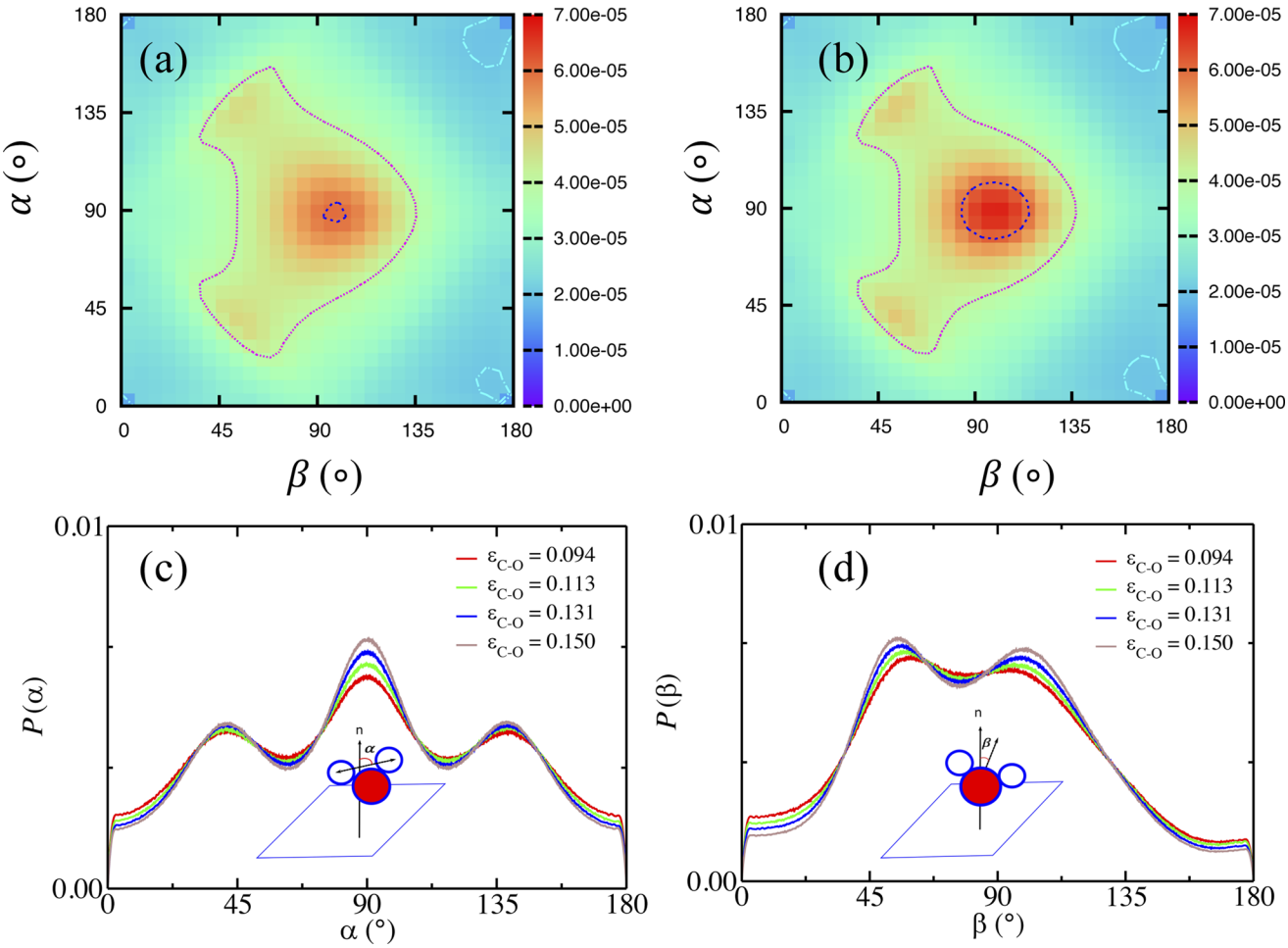

FIG. 4. Probability distributions of angles α and β of water molecules in the first layer of the droplet having (a) the usual interaction and (b) the 60% enhanced LJ interaction. The probability distributions of α and β in the water droplets are shown in (c) and (d), respectively.

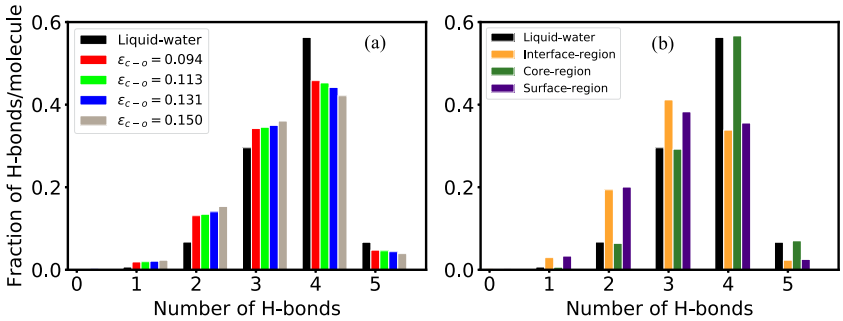

FIG. 5. (a) Fraction of the number of HBs in water droplets and liquid water. The red bars correspond to the usual graphene–water interaction, and the green, blue, and brown bars correspond to the graphene–water systems with 20%, 40%, and 60% enhanced LJ interaction potentials, respectively. (b) Fraction of the number of HBs formed by water molecules in the interface, core, and surface regions of the water droplet having the usual interaction with the graphene surface. The result for liquid water is also shown.

Unlike molecules in liquid water, water molecules in a droplet exist in a heterogeneous environment because of the presence of the graphene/water interface and the droplet surface. Therefore, we examine here the HB coordination of water molecules in a water droplet by dividing the water molecules into three regions: interface, surface, and core regions. The interface region is defined by the first layer of the water droplet on the graphene surface, i.e., $z < 8.2$ Å as in Fig. 2. The outermost layer of water molecules above the first layer on the graphene surface is considered as a surface region, while the rest between the interface and surface regions is considered as a core region. The number fractions of water molecules in the three regions of the water droplets with the different surface–water interactions are shown in Table III.

Figure 5(b) shows the fraction of the number of HBs in the three regions of the water droplet having the usual graphene–water interaction (ε_{C-O} = 0.094 kcal/mol). For water molecules in the core region, the distribution of the fraction of HBs is similar to that of liquid water. On the other hand, in the surface and interface regions, the local HB structure is greatly distorted, i.e., the fraction of three-coordinated water molecules (~40%) is higher than that of four-coordinated water molecules, and the fraction of two-coordinated water molecules in these regions (~20%) is much higher than that in the core region and in liquid water (~7%).

To elucidate the local structure of the water droplets, it is further analyzed in terms of the tetrahedral order parameter q defined as[51]

$$q_i = 1 - \frac{3}{8}\sum_{j=1}^{3}\sum_{k=j+1}^{4}\left(\cos\psi_{j,i,k} + \frac{1}{3}\right)^2, \quad (1)$$

where $\psi_{j,i,k}$ is the angle formed by lines joining the oxygen atom of water molecule i and its four nearest-neighbor oxygen atoms of molecules j and k. This is an index quantifying the similarity of the water structure to the perfect tetrahedral structure: A perfect tetrahedral structure yields $q = 1$, while the value of q decreases as the local structure is distorted from tetrahedral.

Figure 6(a) shows the tetrahedral order parameter of water molecules in water droplets and liquid water. The large q values ($q > 0.7$) for liquid water indicate a locally tetrahedral arrangement of water molecules. In addition, the shoulder at $q \sim 0.5$ arises from a disordered local structure due to HB defects in the system. By contrast, in the water droplet, the fraction of water molecules with a locally distorted tetrahedral structure increases remarkably, i.e., the distribution is small (large) for $q > 0.6$ ($q < 0.6$) and has a long tail even for $q < 0$. Figure 6(a) also shows that the peak of the distribution at $q \sim 0.7$ decreases and shifts to ~0.5 with increasing water–graphene interaction.

To investigate the origin of the distortions of the local structure in the water droplets, we examine the local tetrahedral structure of water molecules in three regions. Figure 6(b) shows the distribution of q in a water droplet having the usual graphene–water interaction. The distribution of q in the core region is almost identical to that of liquid water, as shown by the fraction of the number of HBs in Fig. 5(b). In contrast to the local structure in the core region, the local tetrahedral structure is found to be greatly distorted in the surface region: The distribution for $q > 0.5$ is weakened and has a long tail for $q < 0$ owing to the increase in the number of HB defect molecules with less than four-coordination compared with the distribution in the core region. The present result shows that the distribution for $q > 0.7$ in the interface region is less than that in the surface region, indicating that the local tetrahedral structure is further distorted.

TABLE III. Number fraction of water molecules in different regions inside the water droplets.

Water droplet LJ potential (kcal/mol)	Number fraction of water		
	Interface region	Core region	Surface region
ε_{C-O} = 0.094	0.163	0.505	0.331
ε_{C-O} = 0.113	0.215	0.468	0.318
ε_{C-O} = 0.131	0.278	0.398	0.323
ε_{C-O} = 0.150	0.351	0.313	0.336

B. Vibrational density of states of water droplet

Next, we investigate the dynamics of the water droplets. First, we examine the intermolecular vibrational density of states (vDOS)

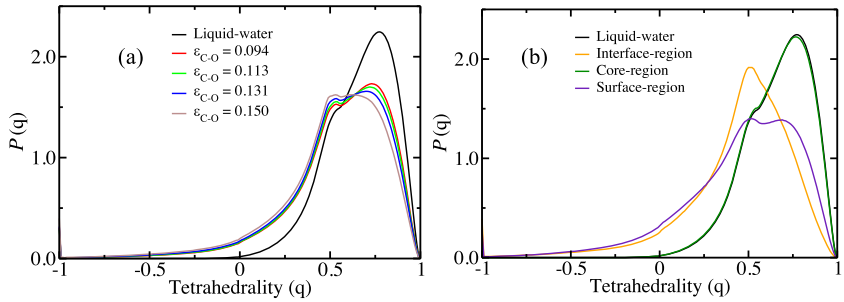

FIG. 6. (a) Probability distributions of the tetrahedral order parameter in a water droplet with different graphene–water interactions and liquid water. The color coding represents the increment in the LJ potential between the surface and water droplet, with red corresponding to the case of usual interaction with the surface. (b) Region-wise tetrahedral order parameter of water molecules in a water droplet with the usual interaction with the graphene surface. The tetrahedral order parameter of liquid water is also shown.

calculated from the Fourier transform of the velocity time correlation function (TCF). Intermolecular vibration motions have intensively been studied by far-IR, Raman, and neutron scattering experiments.[1,52,53] Below 400 cm^{-1}, two peaks are observed at ~60 and ~200 cm^{-1}. These peaks at ~60 and ~200 cm^{-1} have been assigned to the O–O–O HB bending and O–O HB stretching motion, respectively.[1,52,53] There is a general consensus about the origin of the band at ~200 cm^{-1}, whereas there is some debate about the origin of the band at ~60 cm^{-1}.[54,55] On the other hand, above ~400 cm^{-1}, a broad band extending to ~1000 cm^{-1} is observed.[1,52,53] Note that three bands are found in Raman spectroscopy.[1,52,56] The band from ~400 to ~1000 cm^{-1} is assigned to the libration motion. Figure 7(a) shows the vDOS of the oxygen and hydrogen atoms in the water droplets and liquid water. It is known that in liquid water, the vDOS of the oxygen atom has two characteristic peaks at ~60 and ~230 cm^{-1} and the vDOS of the hydrogen atom has a main peak at ~520 cm^{-1} and a weak shoulder at ~900 cm^{-1}, as shown in a previous study.[57] In the water droplets, the three main intermolecular motions are redshifted to ~50, ~200, and ~500 cm^{-1} in the vDOS of the oxygen and hydrogen atoms, respectively, and the vDOS intensities at ~200 and ~50 cm^{-1} are, respectively, weakened and enhanced compared with the vDOS of liquid water. In contrast to the difference between the vDOS of liquid water and water droplets, those between the vDOS of water droplets with different interactions are small.

To elucidate the difference between the vDOS of the water droplets and liquid water, we examine the vDOS of water molecules in the three regions of the water droplet having the usual graphene–water interaction. As can be seen from Fig. 7(b), the vDOSs of the oxygen and hydrogen atoms of water molecules in the core region are almost identical to those in liquid water. On the other hand, those in the interface and surface regions are very different from those in liquid water. In the interface region, the peak of the HB stretching motion is shifted to ~200 cm^{-1}, and the vDOS intensity from ~70 to ~150 cm^{-1} increases. In the surface region, the HB stretching peak is shifted to ~200 cm^{-1}, and an increase in the vDOS intensity is found at lower frequencies, i.e., below ~50 cm^{-1}. The vDOS of the hydrogen atoms in the interface and surface regions shows a redshift in the librational motion, except for the core region. Furthermore, the shoulder peak at ~900 cm^{-1} becomes very weak in these regions. The larger redshift of the HB stretching in the surface region is attributed to the absence of water molecules outside the region.

As we have observed that the fraction of HB defects increases in the interface and surface regions, we investigate the HB number dependence of the vDOS in three regions of the water droplet having the usual water–graphene interaction. Figures 8(a)–8(c) show the vDOS of the two-, three-, and four-coordinated water molecules in three regions of the water droplet. Water molecules in the core region are almost the same as those in liquid water regardless of the number of HBs. It is found that the vDOS intensity at ~200 cm^{-1} is weakened and that at ~50 cm^{-1} it is enhanced with decreasing HB number from four in all the regions. Furthermore, the peak position of the vDOS at ~50 cm^{-1} is found to exhibit a redshift with

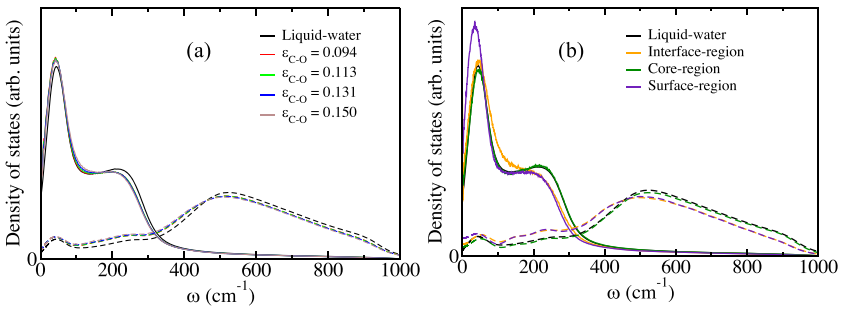

FIG. 7. (a) vDOS of the oxygen (solid lines) and hydrogen (dashed lines) atoms in the water droplets and liquid water. (b) Region-wise vibrational vDOS of the oxygen (solid lines) and hydrogen (dashed lines) atoms of water molecules in the liquid water and water droplets having the usual interaction with the graphene surface. The vDOSs of the oxygen and hydrogen atoms in liquid water are also shown.

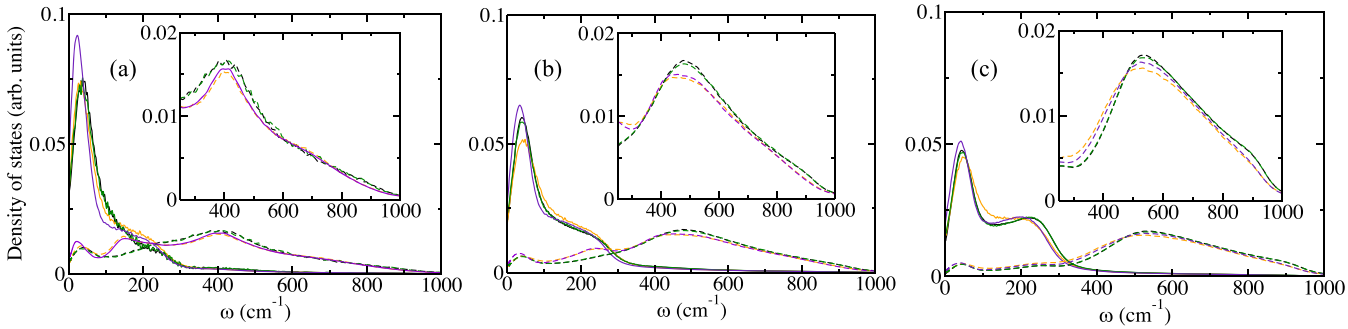

FIG. 8. vDOS of the oxygen (solid lines) and hydrogen (dashed lines) atoms of (a) two-, (b) three-, and (c) four-coordinated water molecules in different regions of the water droplet. The black, yellow, green, and violet lines are the vDOSs of the liquid water, interface, core, and surface regions, respectively. The vDOSs of the libration motion are expanded in the inset.

decreasing HB number. The changes in the intensity of the vDOS at ~50 and ~200 cm^{-1} and the redshift of the band at ~50 cm^{-1} are larger in the interface region and especially in the surface region.

In the case of hydrogen atoms, the vDOS of those in the core region of the water droplet is almost identical to that of liquid water irrespective of the HB number. It should be noted that the vDOSs of hydrogen atoms, even those of the water molecules with four HBs in the interface and surface regions, are distorted toward low frequencies, i.e., the vDOSs in the interface and surface regions are weakened on the high-frequency side and strengthened on the low-frequency side of the main peak of the librational motion. With decreasing HB number, the peak position of the librational motion in each region is shifted to a lower frequency, e.g., ~400 cm^{-1}, and the shoulder peak at ~50 cm^{-1} almost disappears for water molecules with two HBs. It is also worth noting the emergence of a peak at ~250 cm^{-1} in the vDOS of the hydrogen atoms of water molecules with fewer than four HBs is in the interface and surface region. The present results show that the difference between the vDOS of the water droplets and liquid water can be attributed to the presence of the interfaces, particularly the surface region corresponding to the air/water interface, with water molecules having fewer HBs.

To understand the generality of this result, we simulate a water slab system consisting of 1000 water molecules, which is a two-dimensional periodic water structure with the air/water interface in the z dimension. A preliminary result presented in Fig. 9 shows that the vDOS of water molecules at the air/water interface in the water slab system exhibits the same behavior as observed in the vDOS of water molecules in the surface region of the water droplets, whereas the behavior of water molecules in the core region of the water slab system is the same as that in liquid water. A detailed analysis of the water slab system is currently underway and will be published separately.

The present study reveals the redshift of the vDOS of all the intermolecular motions due to the lower numbers of HBs of water molecules in the surface and interface regions of the water droplets. It has been revealed that the energy relaxation dynamics of the O–H stretching and H–O–H bending of a water molecule depend on the number of HBs of the molecule in liquid water, for example, the energy relaxation time of these intramolecular motions of a three-coordinated water molecule is slower (by ~10% to 40%) than that of a four-coordinated water molecule.[58,59] In addition, energy relaxation dynamics can be investigated using pump–probe spectroscopy and by examining the transient changes in vDOS under the application of external fields.[57,59–61] The present study finds that the vDOSs of water molecules in the surface and interface regions are different from those in liquid water. Thus, it is expected that the intermolecular vibrational energy relaxation dynamics at the surface or interface region of a droplet and at a water/air interface will be found to be different from those in liquid water.

C. Orientation relaxation of water droplet

We now investigate single-molecule and collective orientation relaxation in water droplets. The SMOR of a water molecule, $\phi(t)$, is defined as

$$\phi(t) = \frac{\langle \vec{\mu}(t) \cdot \vec{\mu}(0) \rangle}{\langle \mu^2 \rangle}. \quad (2)$$

Here, we calculate the SMOR as the average of all the water molecules in the system. The SMORs in the water droplets and liquid water are shown in Fig. 10(a), and the relaxation times are

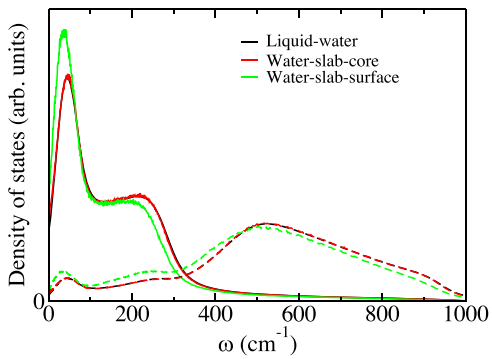

FIG. 9. vDOS of water molecules in different regions of the water slab system. The vDOS of liquid water is also shown.

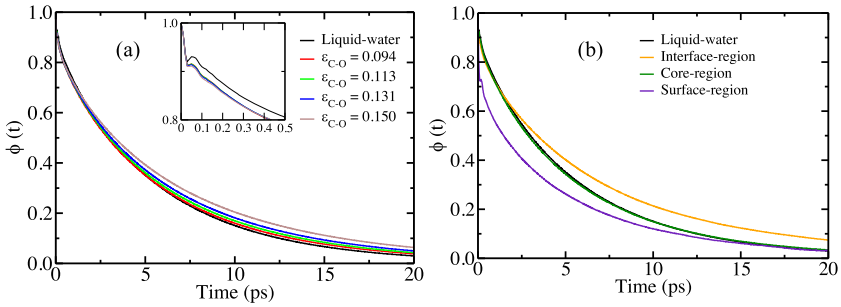

FIG. 10. (a) SMORs in water droplets and liquid water and (b) region-wise SMORs in a water droplet having the usual interaction with the graphene interface. The SMOR in liquid water is also shown.

summarized in Table IV. The present result shows that SMOR in liquid water with a relaxation time of 5.4 ps is slightly faster than in water droplets with a relaxation time of 5.4–6.4 ps. The dynamics of SMOR in a water droplet slows down slightly with increasing water–graphene interaction.

Figure 10(b) shows the SMORs in the three regions of the water droplet having the usual interaction with the graphene surface. It is found that the SMOR in the surface region is the fastest because there are fewer HBs per water molecule and a free boundary is present. On the other hand, the SMOR in the interface region is the slowest because the rotational motion is hindered by the presence of the graphene surface. As mentioned above, the number of water molecules in the interface region increases with increasing water–graphene interaction, and the average SMOR becomes slower with increasing water–graphene interaction.

Next, we investigate the COR of water molecules. The COR $\Phi(t)$ is defined as the normalized TCF of the total dipole moment $\vec{M}$ of the system,

$$\Phi(t) = \frac{\langle \delta\vec{M}(t) \cdot \delta\vec{M}(0) \rangle}{\langle \delta M^2 \rangle}, \tag{3}$$

where $\delta\vec{M}(t)$ is the fluctuation of the total dipole moment of the system, $\vec{M}$, from its mean value $\langle\vec{M}\rangle$, i.e., $\delta\vec{M}(t) = \vec{M}(t) - \langle\vec{M}\rangle$. In this study, we approximate the total dipole moment $\vec{M}$ as the sum of the dipole moments of individual water molecules $\vec{\mu}_i(t)$,

$$\vec{M}(t) = \sum_{i=1}^{N} \vec{\mu}_i(t). \tag{4}$$

Figure 11(a) shows the CORs in the water droplets and liquid water. Compared with SMOR, COR shows a significant difference between water droplets and liquid water. It is known that in liquid water, COR is approximately two times *slower* than SMOR.[62] In the present results, the relaxation times of COR and SMOR in liquid water are ~11.9 and ~5.4 ps, respectively. By contrast, the present study reveals that in a water droplet, COR becomes ~2.5–5 times *faster* than SMOR. Furthermore, the COR of a water droplet having the usual graphene–water interaction is about 11 times faster than that in liquid water. A similar behavior is observed for water confined in spherical nanocavities.[63] In the case of spherical nanocavities, the effect of different interactions and cavity size on COR is almost negligible, whereas in water droplets on graphene, COR becomes sluggish with an increase in interaction with the surface.

TABLE IV. Orientation relaxation times, Kirkwood and dynamic Kirkwood factors, and parallel and perpendicular components of the Kirkwood factor of water droplets and liquid water.

	τ_{COR} (ps)	τ_{SMOR} (ps)	G_K	$\hat{G}_K^D(0)$	$G_{K\parallel}$	$G_{K\perp}$
Liquid water	11.86	5.37	3.23	1.46	3.23	3.23
ε_{C-O} = 0.094	0.90	5.43	0.24	1.45	0.28	0.15
ε_{C-O} = 0.113	1.28	5.63	0.26	1.14	0.32	0.14
ε_{C-O} = 0.131	1.43	5.84	0.30	1.23	0.38	0.13
ε_{C-O} = 0.150	2.25	6.34	0.40	1.13	0.53	0.15

In addition to the significant acceleration of COR in the water droplets, it also shows a large initial decay compared with COR in liquid water. Figure 11(b) shows the absorption spectra of liquid water and water droplets, given by

$$\alpha(\omega) = \omega^2 \int_0^\infty \Phi(t) \cos(\omega t)\, dt. \tag{5}$$

The absorption spectrum of the water droplets shows a considerable blueshift of the librational motion compared with liquid water, which is attributed to the large initial decay of the COR of the droplets.

To understand the difference between the dynamics of the total dipole moment in the water droplets and in liquid water, the COR is divided into two terms,

$$\Phi(t) = \Phi_{self}(t) + \Phi_{cross}(t), \tag{6}$$

where

$$\Phi_{self}(t) = \frac{\left\langle \sum_{i=1}^{N} (\vec{\mu}_i(t) - \langle\vec{M}\rangle) \cdot (\vec{\mu}_i(0) - \langle\vec{M}\rangle) \right\rangle}{\langle \delta M^2 \rangle}, \tag{7}$$

$$\Phi_{cross}(t) = \frac{\left\langle \sum_{i\neq j}^{N} (\vec{\mu}_i(t) - \langle\vec{M}\rangle) \cdot (\vec{\mu}_j(0) - \langle\vec{M}\rangle) \right\rangle}{\langle \delta M^2 \rangle}. \tag{8}$$

Here, $\Phi_{self}(t)$ is proportional to the SMOR given in Eq. (2).

Figure 12(a) shows that in liquid water, $\Phi_{cross}(t)$ is positive and slower than $\Phi_{self}(t)$, and thus, COR is slower than SMOR. On the other hand, as shown in Fig. 12(b), in the water droplets,

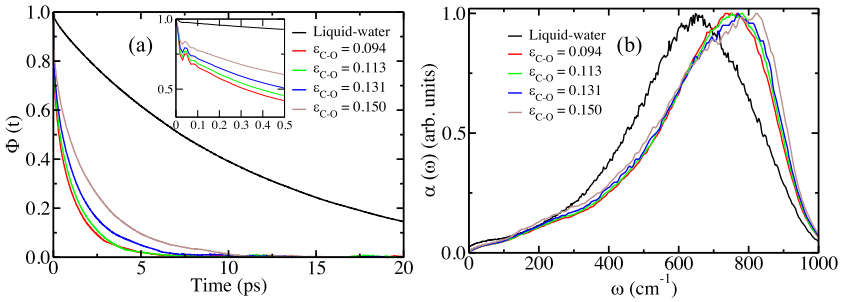

FIG. 11. (a) COR and (b) far-infrared absorption spectra of water droplets and liquid water. The absorption spectra are normalized based on their respective librational peaks.

$\Phi_{cross}(t)$ and $\Phi_{self}(t)$ have opposite signs, which leads to cancellation of these terms. As a result, in the water droplets, COR is faster than SMOR.

Figure 13 shows the absorption spectra corresponding to the self- and cross-terms of liquid water and a water droplet having the usual water–graphene interaction. The absorption spectrum of the self-term of the water droplet is very similar to that of liquid water. However, we find large differences between the spectra of the cross-term of the water droplet and liquid water, for instance, in the water droplet, a positive and a negative peak are found at ~750 and at ~480 cm^{-1}, respectively, whereas in liquid water, a positive peak and two negative peaks are found at ~650 and at ~480 and ~900 cm^{-1}, respectively. Consequently, the differences between the distinct correlation of the dipole moments in the water droplets and liquid water give rise to significant differences between the TCFs and spectra of these systems. It is noted that the blueshift in the libration motion of the water droplets is due to the dipole cross correlations, not the stiffness of the water interaction.

A difference between the correlations of dipole moments is found in a static quantity, namely, the Kirkwood g-factor, G_K. Since it is known that the convergence of dielectric properties is slow,[64] we have ensured that the reported G_K values in this work are converged in the time limit of our simulation (see Fig. S1 of the supplementary material). As summarized in Table IV, in liquid water, G_K is greater than three, which indicates a constructive correlation of dipole moments of water molecules ($\langle \delta M^2 \rangle > N\langle \mu^2 \rangle$, i.e., there is a positive correlation between distinct dipole moments). On the other hand, in water droplets, G_K is found to be less than unity owing to a destructive correlation of dipole moments ($\langle \delta M^2 \rangle < N\langle \mu^2 \rangle$, i.e., there is a negative correlation between distinct dipole moments). Because the magnitude of the total dipole moment is smaller than the sum of individual dipole moments in a water droplet, the collective dipole moment is sensitive to the fluctuation of an individual dipole moment, as found in an isolated water cluster.[62] The small value of G_K in the presence of an interface is responsible for a low value of static dielectric constant ε_0.[65–67] Thus, we also expect small ε_0 for the water droplets, although ε_0 for water droplet is not unambiguously determined owing to its irregular shape.

Furthermore, a relation between the relaxation time of the COR, τ_{COR}, and that of the SMOR, τ_{SMOR}, can be derived using G_K, based on the Mori–Zwanzig equation for the dipole moment correlation matrix,[68]

$$\tau_{COR} = \frac{G_K}{\hat{G}_K^D(0)}\,\tau_{SMOR}, \tag{9}$$

where

$$G_K = \frac{\langle \delta M^2 \rangle}{N\langle \mu^2 \rangle}, \tag{10}$$

$$\hat{G}_K^D(\omega) = \frac{\int_0^\infty dt\, e^{-i\omega t} \left\langle \delta \dot{\vec{M}}(t) \cdot \delta \dot{\vec{M}}(0) \right\rangle_Q}{\int_0^\infty dt\, e^{-i\omega t} \sum_{i=1}^N \left\langle \dot{\vec{\mu}}_i(t) \cdot \dot{\vec{\mu}}_i(0) \right\rangle_Q}. \tag{11}$$

Here, $\hat{G}_K^D(0)$ is a dynamical analog of G_K, expressing the correlation in the memory function of the collective orientation relative to that of individual orientations, and the subscript Q in $\hat{G}_K^D$ denotes the time evolution in projected space. It is expected that $\hat{g}_K^D(0)$ is close to unity because of the ratio of fast dynamics of the memory function. As mentioned above, a constructive correlation between dipole moments is found in liquid water, $G_K > 1$, and thus, the relaxation time of COR is much longer than that of SMOR in liquid water. On the other hand, a destructive correlation, $G_K < 1$, is found in water

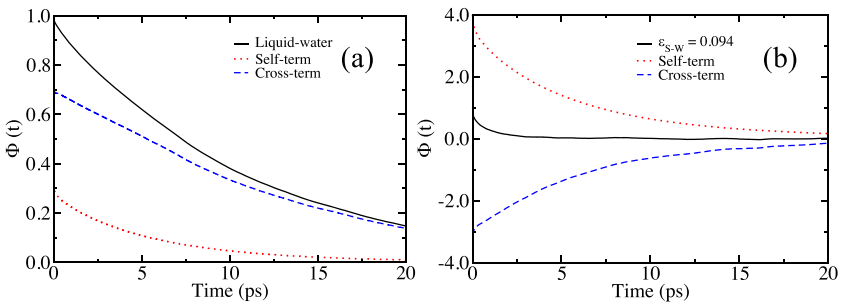

FIG. 12. Self-correlations (dotted line) and cross correlations (dashed line) of the CORs in (a) liquid water and (b) a water droplet having the usual interaction with the graphene surface.

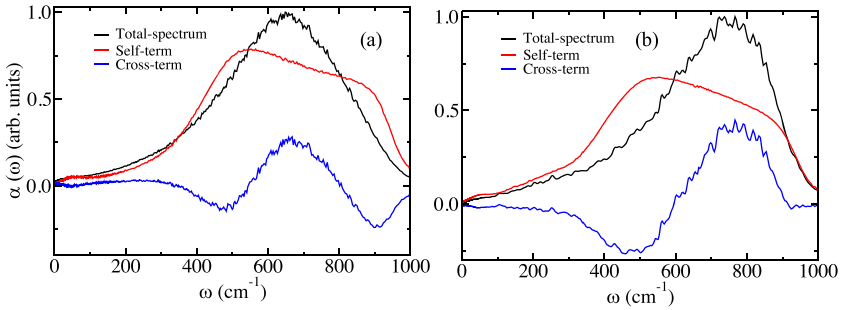

FIG. 13. Self- and cross-terms of the far-infrared spectrum of (a) liquid water and (b) a water droplet having the usual interaction with the graphene surface. The absorption spectra are normalized based on their respective librational peaks.

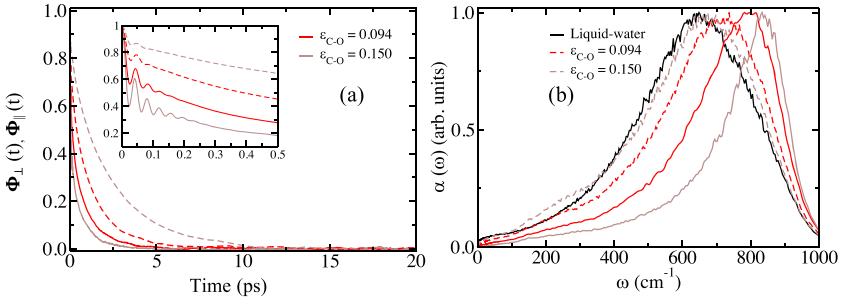

FIG. 14. (a) Parallel (dashed line) and perpendicular (solid line) components of the COR of water droplets having the usual and 60% interactions with the graphene surface. (b) The corresponding far-infrared absorption spectra of liquid water and water droplets. The absorption spectra are normalized based on their respective librational peaks.

droplets. As a result, in water droplets, COR becomes faster than SMOR. A similar acceleration mechanism of COR is found in water clusters and confined water molecules.[62,69]

Table IV shows that the Kirkwood factor gradually increases with increasing water–graphene interaction. To understand the effect of the water–solid and water–air interactions, we analyze the parallel and perpendicular components, $G_{K,\parallel}$ and $G_{K,\perp}$, of the Kirkwood factor with respect to the graphene surface,

$$G_K = \tfrac{1}{3}(2G_{K\parallel} + G_{K\perp}), \tag{12}$$

where

$$G_{K\parallel} = \frac{3\langle M_\parallel^2\rangle}{N\langle\mu^2\rangle}, \tag{13}$$

$$G_{K\perp} = \frac{3\langle M_\perp^2\rangle}{N\langle\mu^2\rangle} \tag{14}$$

with $\langle M_\parallel^2\rangle = \frac{1}{2}\langle M_x^2 + M_y^2\rangle$ and $\langle M_\perp^2\rangle = \langle M_z^2\rangle$. The perpendicular component of the dipole moment is in the direction of the surface normal vector.

We find that the total dipole moments along the z axis in the interface and surface regions are largely canceled, and $G_{K\perp}$ is almost independent of the water–graphene interaction. On the other hand, we also find that $G_{K\parallel}$ gradually increases with increasing water–graphene interaction. As a result, G_K increases with increasing water–graphene interaction. A small fluctuation in the perpendicular component of the total dipole moment is also found in the nanoconfined water between graphene sheets.[66]

We now examine the TCFs of the parallel and perpendicular components of the total dipole moment in water droplets. It should be noted that these TCFs are similar within statistical error in liquid water. Figure 14(a) shows that the TCF of the perpendicular component, $\Phi_\perp(t)$, is faster than that of the parallel component, $\Phi_\parallel(t)$, in water droplets, for example, $\tau_\perp \sim 0.68$ ps (0.64 ps) and $\tau_\parallel \sim 1.00$ ps (2.17 ps) in a water droplet having the usual (60% enhanced) interaction. It is noted that an increase in the water–graphene interaction does not significantly change $\tau_\perp$, whereas it largely changes $\tau_\parallel$. The interaction dependency of $\tau_\perp$ and $\tau_\parallel$ is attributed to the change in $G_{K\perp}$ and $G_{K\parallel}$ with a change in water–graphene interaction. Furthermore, $\Phi_\perp(t)$ exhibits more pronounced oscillations than $\Phi_\parallel(t)$. This is also due to the negative correlation between distinct dipole moments, i.e., a small G_K makes the total dipole moment more susceptible to the fluctuations of individual dipole moments. Similar rapid and pronounced oscillations are found in the perpendicular component of a nanoconfined water system.[66] As a result, the libration peak in the absorption spectrum of the perpendicular component in a water droplet is shifted to a higher frequency than those in the parallel component and in liquid water [Fig. 14(b)].

IV. CONCLUSIONS

In this study, we investigated the structural and dynamic properties of water droplets on a graphene surface by performing MD simulations. First, we studied the local structure of the water droplets in terms of HB number per molecule and the tetrahedral order parameter. In particular, we examined these properties of water droplets by dividing the system into three regions: a (water/solid) interface region, a core region, and a surface (water/air interface) region. We found that the local structure of water molecules in the core region is very similar to that in liquid water. However, the

present study has revealed that the local structure is greatly distorted in the interface and surface regions owing to the presence of the water/solid and water/air interfaces: three-coordinated water molecules are the most abundant, and thus, the local structure is distorted from tetrahedral. Furthermore, we found the change in the structure of the water droplets on the graphene surface as the interaction with the surface increases, i.e., the decrease in contact angle corresponding to the spreading of water molecules on the surface. In addition, we found that the local structure becomes less ordered with increasing water–graphene interaction.

We investigated the dynamics of water droplets by calculating the intermolecular vibrational vDOS. It was revealed that the vDOS at ~50 cm^{-1} increased and that at ~200 cm^{-1} decreased in the surface and interface regions. We also found that the librational motion of the hydrogen atoms in the surface and interface regions was redshifted compared with that of liquid water. We found that the changes in the vDOS of the droplets compared with that of liquid water are due to there being fewer hydrogen-bonded water molecules, such as three- and two-coordinated water molecules, in the interface and surface regions of the water droplets. These results suggest that the energy relaxation dynamics in a water droplet, especially in the surface and interface regions, can be different from those in liquid water. In addition, we found that the vDOS of the intermolecular translational and librational motions of molecules in the surface region of a water slab system is very similar to that of water molecules in the surface region of a water droplet. Thus, the present results imply slower intermolecular energy relaxation dynamics at the water/air interface compared with the bulk.

We also studied both single-molecule and collective orientation relaxations of water droplets. We found that SMOR of water droplets is slightly slower than that of liquid water. We also found that COR is faster than SMOR in water droplets and that it is more than 11 times faster in droplets than in liquid water. This is due to the negative correlation between different dipole moments in water droplets, as shown by the Mori–Zwanzig equation. The present analysis also showed that the negative correlation of the distinct dipole moments yields a blueshift of the librational motion in the far-infrared spectrum of water droplets, compared with that of liquid water. It is of great importance to recognize that this blueshift of the librational motion is due to the negative correlation between dipole moments, not to a stiffer intermolecular interaction. Furthermore, the present study showed that SMOR slows down slightly with increasing water–graphene interaction. In addition, we found that with increasing interaction, the Kirkwood g-factor, i.e., the correlation between dipole moment, increases, although still less than one, and COR slows down.

We examined the parallel and perpendicular components of the total dipole moments, and we observed pronounced oscillations of the perpendicular component due to the large cancellation of the total dipole moment. A similar behavior is found in nanoconfined systems. It is therefore expected that the differences in dynamical behavior between water molecules in liquid water and in the surface regions of water droplets will also be observed in other systems in which air/water interfaces are present. Furthermore, we found that with the increase in water graphene interaction, oscillations in the perpendicular component become apparent and the increase in blueshift in the spectrum of the perpendicular component as well as the slowdown of relaxation time of the parallel component is observed.

The intermolecular dynamics of water molecules at interfaces are not well understood. Therefore, it is of interest to investigate the intermolecular translational and orientational dynamics of water molecules in these systems both experimentally and theoretically.

SUPPLEMENTARY MATERIAL

We have provided a figure in the supplementary material to show the convergence of the G_K factor in our simulation.

ACKNOWLEDGMENTS

This work was supported by the Grant-in-Aid for Scientific Research (Grant Nos. JP16H02254 and JP21H04676 to S.S.) from JSPS. M.M. would like to thank Dr. Inagaki and Ms. Prerna for valuable discussion. Computational facilities are provided by the Research Center for Computational Sciences in Okazaki.

DATA AVAILABILITY

The data that support the findings of this study are available from the corresponding author upon reasonable request.

REFERENCES

[1] D. Eisenberg and W. Kauzmann, *The Structure and Properties of Water* (Oxford University Press, 2005).
[2] B. Bagchi, *Water in Biological and Chemical Processes: From Structure and Dynamics to Function*, Cambridge Molecular Science (Cambridge University Press, 2013).
[3] C. A. Angell, W. J. Sichina, and M. Oguni, J. Phys. Chem. **86**, 998 (1982).
[4] P. H. Poole, F. Sciortino, U. Essmann, and H. E. Stanley, J. Phys. Chem. B **360**, 324 (1992).
[5] O. Mishima and H. E. Stanley, J. Phys. Chem. **396**, 329 (1998).
[6] J. C. Palmer, F. Martelli, Y. Liu, R. Car, A. Z. Panagiotopoulos, and P. G. Debenedetti, Nature **510**, 385 (2014).
[7] P. Gallo, K. Amann-Winkel, C. A. Angell, M. A. Anisimov, F. Caupin, C. Chakravarty, E. Lascaris, T. Loerting, A. Z. Panagiotopoulos, J. Russo, J. A. Sellberg, H. E. Stanley, H. Tanaka, C. Vega, L. Xu, and L. G. M. Pettersson, Chem. Rev. **116**, 7463 (2016).
[8] S. Saito, B. Bagchi, and I. Ohmine, J. Chem. Phys. **149**, 124504 (2018).
[9] E. B. Moore and V. Molinero, J. Chem. Phys. **130**, 244505 (2009).
[10] J. Russo and H. Tanaka, Nat. Commun. **5**, 3556 (2014).
[11] A. Nilsson and L. G. M. Pettersson, Nat. Commun. **6**, 8998 (2015).
[12] J. C. Palmer, P. H. Poole, F. Sciortino, and P. G. Debenedetti, Chem. Rev. **118**, 9129 (2018).
[13] J. W. Biddle, R. S. Singh, E. M. Sparano, F. Ricci, M. A. González, C. Valeriani, J. L. F. Abascal, P. G. Debenedetti, M. A. Anisimov, and F. Caupin, J. Chem. Phys. **146**, 034502 (2017).
[14] N. Moritsugu, T. Nara, S.-i. Koda, K. Tominaga, and S. Saito, J. Phys. Chem. B **124**, 11730 (2020).
[15] U. Heugen, G. Schwaab, E. Bründermann, M. Heyden, X. Yu, D. M. Leitner, and M. Havenith, Proc. Natl. Acad. Sci. U. S. A. **103**, 12301 (2006).
[16] S. Park and M. D. Fayer, Proc. Natl. Acad. Sci. U. S. A. **104**, 16731 (2007).
[17] A. P. Gaiduk and G. Galli, J. Phys. Chem. Lett. **8**, 1496 (2017).
[18] P. Schienbein, G. Schwaab, H. Forbert, M. Havenith, and D. Marx, J. Phys. Chem. Lett. **8**, 2373 (2017).
[19] F. Merzel and J. C. Smith, Proc. Natl. Acad. Sci. U. S. A. **99**, 5378 (2002).

[20]S. K. Pal and A. H. Zewail, Chem. Rev. **104**, 2099 (2004).
[21]Y. R. Shen and V. Ostroverkhov, Chem. Rev. **106**, 1140 (2006).
[22]M. Bonn, Y. Nagata, and E. H. G. Backus, Angew. Chem., Int. Ed. **54**, 5560 (2015).
[23]S. Nihonyanagi, S. Yamaguchi, and T. Tahara, Chem. Rev. **117**, 10665 (2017).
[24]T. Ishiyama and A. Morita, Annu. Rev. Phys. Chem. **68**, 355 (2017).
[25]Y. Nagata, C.-S. Hsieh, T. Hasegawa, J. Voll, E. H. G. Backus, and M. Bonn, J. Phys. Chem. Lett. **4**, 1872 (2013).
[26]Y. Tong, T. Kampfrath, and R. K. Campen, Phys. Chem. Chem. Phys. **18**, 18424 (2016).
[27]F. H. Song, B. Q. Li, and C. Liu, Langmuir **29**, 4266 (2013).
[28]C. D. Daub, D. Bratko, K. Leung, and A. Luzar, J. Phys. Chem. C **111**, 505 (2007).
[29]F. Cyriac, P. M. Lugt, and R. Bosman, Tribol. Trans. **59**, 679 (2016).
[30]T. Kajiya, F. Schellenberger, P. Papadopoulos, D. Vollmer, and H.-J. Butt, Sci. Rep. **6**, 23687 (2016).
[31]J. Jang, G. C. Schatz, and M. A. Ratner, Phys. Rev. Lett. **90**, 156104 (2003).
[32]C. E. Cansoy, RSC Adv. **4**, 1197 (2014).
[33]J. Drelich, J. D. Miller, and R. J. Good, J. Colloid Interface Sci. **179**, 37 (1996).
[34]J. D. Bernardin, I. Mudawar, C. B. Walsh, and E. I. Franses, Int. J. Heat Mass Transfer **40**, 1017 (1997).
[35]K.-Y. Yeh, L.-J. Chen, and J.-Y. Chang, Langmuir **24**, 245 (2008).
[36]T. G. Twardeck, IBM J. Res. Dev. **21**, 31 (1977).
[37]M. Barletta and A. Gisario, Prog. Org. Coat. **64**, 339 (2009).
[38]E. Schäffer, T. Thurn-Albrecht, T. P. Russell, and U. Steiner, Nature **403**, 874 (2000).
[39]W. D. Luedtke, J. Gao, and U. Landman, J. Phys. Chem. C **115**, 20343 (2011).
[40]J. L. F. Abascal and C. Vega, J. Chem. Phys. **123**, 234505 (2005).
[41]W. D. Cornell, P. Cieplak, C. I. Bayly, I. R. Gould, K. M. Merz, D. M. Ferguson, D. C. Spellmeyer, T. Fox, J. W. Caldwell, and P. A. Kollman, J. Am. Chem. Soc. **117**, 5179 (1995).
[42]W. Wang, H. Zhang, S. Li, and Y. Zhan, Nanotechnology **27**, 075707 (2016).
[43]T. Werder, J. H. Walther, R. L. Jaffe, T. Halicioglu, and P. Koumoutsakos, J. Phys. Chem. B **107**, 1345 (2003).
[44]S. Plimpton, J. Comput. Phys. **117**, 1 (1995).
[45]M. J. de Ruijter, T. D. Blake, and J. De Coninck, Langmuir **15**, 7836 (1999).
[46]R. C. Dutta, S. Khan, and J. K. Singh, Fluid Phase Equilib. **302**, 310 (2011).
[47]J. Włoch, A. P. Terzyk, and P. Kowalczyk, Chem. Phys. Lett. **674**, 98 (2017).
[48]A. Pertsin and M. Grunze, J. Phys. Chem. B **108**, 1357 (2004).
[49]J. Marti, G. Nagy, M. C. Gordillo, and E. Guàrdia, J. Chem. Phys. **124**, 094703 (2006).
[50]A. Luzar and D. Chandler, J. Chem. Phys. **98**, 8160 (1993).
[51]J. R. Errington and P. G. Debenedetti, Nature **409**, 318 (2001).
[52]G. E. Walrafen, in *Water: Comprehensive Treatise*, edited by F. Franks (Plenum, New York, 1972), Chap. 1, p. 151.
[53]D. I. Page, in *Water: Comprehensive Treatise*, edited by F. Franks (Plenum, New York, 1972), Chap. 1, p. 333.
[54]J. A. Padró and J. Martí, J. Chem. Phys. **118**, 452 (2003).
[55]J. Martí, J. A. Padró, and E. Guàrdia, J. Chem. Phys. **105**, 639 (1996).
[56]M. Moskovits and K. H. Michaelian, J. Chem. Phys. **69**, 2306 (1978).
[57]T. Yagasaki and S. Saito, J. Chem. Phys. **134**, 184503 (2011).
[58]B. Miguel, J. Zúñiga, A. Requena, and A. Bastida, J. Phys. Chem. B **118**, 9427 (2014).
[59]S. Imoto, S. S. Xantheas, and S. Saito, J. Phys. Chem. B **119**, 11068 (2015).
[60]T. Yagasaki and S. Saito, Annu. Rev. Phys. Chem. **64**, 55 (2013).
[61]J. Jeon and M. Cho, J. Chem. Phys. **135**, 214504 (2011).
[62]S. Saito and I. Ohmine, J. Chem. Phys. **101**, 6063 (1994).
[63]S. Mondal, S. Acharya, and B. Bagchi, Phys. Rev. Res. **1**, 033145 (2019).
[64]M. Neumann, J. Chem. Phys. **85**, 1567 (1986).
[65]S. Senapati and A. Chandra, J. Phys. Chem. B **105**, 5106 (2001).
[66]S. Mondal and B. Bagchi, J. Chem. Phys. **154**, 044501 (2021).
[67]L. Fumagalli, A. Esfandiar, R. Fabregas, S. Hu, P. Ares, A. Janardanan, Q. Yang, B. Radha, T. Taniguchi, K. Watanabe, G. Gomila, K. S. Novoselov, and A. K. Geim, Science **360**, 1339 (2018).
[68]D. Kivelson and P. Madden, Mol. Phys. **30**, 1749 (1975).
[69]R. Biswas and B. Bagchi, J. Chem. Phys. **133**, 084509 (2010).